PHYSICAL REVIEW B **95**, 020503(R) (2017)

Tuning phase transitions in FeSe thin flakes by field-effect transistor with solid ion conductor as the gate dielectric

B. Lei,[1] N. Z. Wang,[1] C. Shang,[1] F. B. Meng,[1] L. K. Ma,[1] X. G. Luo,[1,2] T. Wu,[1,2] Z. Sun,[2,3] Y. Wang,[4] Z. Jiang,[4] B. H. Mao,[5] Z. Liu,[5,6] Y. J. Yu,[7] Y. B. Zhang,[2,7,*] and X. H. Chen[1,2,8,†]

[1]*Hefei National Laboratory for Physical Sciences at Microscale and Department of Physics, and CAS Key Laboratory of Strongly-coupled Quantum Matter Physics, University of Science and Technology of China, Hefei, Anhui 230026, China*

[2]*Collaborative Innovation Center of Advanced Microstructures, Nanjing University, Nanjing 210093, China*

[3]*National Synchrotron Radiation Laboratory, University of Science and Technology of China, Hefei, Anhui 230026, China*

[4]*Shanghai Institute of Applied Physics, Chinese Academy of Sciences, Shanghai 201204, China*

[5]*State Key Laboratory of Functional Materials for Informatics, Shanghai Institute of Microsystem and Information Technology, Chinese Academy of Sciences, Shanghai 200050, China*

[6]*School of Physical Science and Technology, Shanghai Tech University, Shanghai 200031, China*

[7]*State Key Laboratory of Surface Physics and Department of Physics, Fudan University, Shanghai 200433, China*

[8]*High Magnetic Field Laboratory, Chinese Academy of Sciences, Hefei, Anhui 230031, China*

(Received 25 September 2016; revised manuscript received 6 November 2016; published 30 January 2017)

We have developed a field-effect transistor (FET) device using a solid ion conductor (SIC) as the gate dielectric, which can tune the carrier density of FeSe by driving lithium ions in and out of the FeSe thin flakes and consequently control the physical properties and phase transitions. A dome-shaped superconducting phase diagram was mapped out with increasing Li content, with $T_c \sim 46.6$ K for optimal doping, and an insulating phase was reached at the extremely overdoped regime. Our study suggests that, by using a solid ion conductor as the gate dielectric, the SIC-FET device is able to induce much higher carrier doping in the bulk, suit many surface-sensitive experimental probes, and stabilize structural phases that are inaccessible in ordinary conditions.

DOI: 10.1103/PhysRevB.95.020503

Chemical doping is a conventional way to introduce charge carriers into solids. This approach has led to the finding of high-T_c superconductivity in cuprates and iron-based superconductors by suppressing antiferromagnetism or the spin density wave with a chemical doping of $\sim$10% or $\sim 10^{21}$ dopant per cm^3 [1–3]. However, the element replacement and the variation in carrier density cannot practically cover a large regime and therefore leaves many phases unexplored. As a complementary method, the application of field-effect transistors (FETs) in two-dimensional systems is an effective way to control electronic properties via reversible changes in charge carrier density [4–18]. Such an electrostatic doping is desirable to study phases that cannot be achieved by material synthetic methods [7,9–11,13,15,16,18]. FET devices have been widely applied in the exploration of new superconductors [10,11], the preparation for new devices [19,20], as well as many applications in the semiconductor industry [7].

So far, only two types of FET devices, metal-insulator-semiconductor (MIS) FET [Fig. 1(a)] and electric double-layer (EDL) FET [Fig. 1(b)], have been widely used to continuously tune the carrier density [21,22]. In conventional MIS-FET devices, electrostatic doping to a system is realized by the accumulation of mobile carriers at the surface of an insulator with an applied gate voltage [6,7,11,21,22]. A limited sheet carrier density n_{2D} of $\sim 1 \times 10^{13}$ cm^{-2} can be obtained on the surface of an insulator before the gate dielectric breaks down due to a large electric field [5,9,11]. They cannot provide sufficient carriers to induce superconductivity [22]. The EDL-FET with a liquid electrolyte as the gate dielectric can achieve a higher two-dimensional carrier density n_{2D} of $\sim 8 \times 10^{14}$ cm^{-2} [23]. However, the overlay of a liquid electrolyte makes it difficult to be implemented in modern electronic technology and prevents the device from being characterized by many physical measurements. In addition, many materials of interest have an electrochemical reaction with the liquid electrolyte [24,25]. Moreover, both FETs can only tune the accumulation of the carrier on the surface of materials. We have recently designed an ionic field-effect transistor (iFET) with a gel-like electrolyte as the gate medium and modulated 1T-TaS_2 electronic properties by tunable Li ion intercalation [12]. In this Rapid Communication, by using a solid ion conductor (SIC) as the gate dielectric, we introduce a different type of FET, SIC-FET [Fig. 1(c)]. This type of FET device exposes sample surfaces for surface-sensitive experimental probes and tunes material properties by driving Li ions in and out of layered samples. This configuration naturally solves the shortcoming of the carrier control methods mentioned above and can pave the way for the investigation of different electronic states in solids.

To demonstrate the capability of the SIC-FET device, we choose FeSe as a model material. FeSe has the simplest structure of iron-based high-temperature superconductors, with conducting FeSe layers stacked along the c axis [26]. FeSe and its derived superconductors are currently the focus of research in the field of iron-based superconductors [27–31]. In particular, the monolayer FeSe thin film on a $SrTiO_3$ substrate has generated wide research interest because of its unexpectedly high-T_c superconductivity with a T_c as high as 65 K, in sharp contrast to the bulk $T_c < 10$ K [27,31–36]. Numerous studies have shown that those FeSe-derived materials with $T_c > 40$ K are heavily electron-doped systems, which share very similar electronic structures [37,38]. The

*zhyb@fudan.edu.cn
†chenxh@ustc.edu.cn

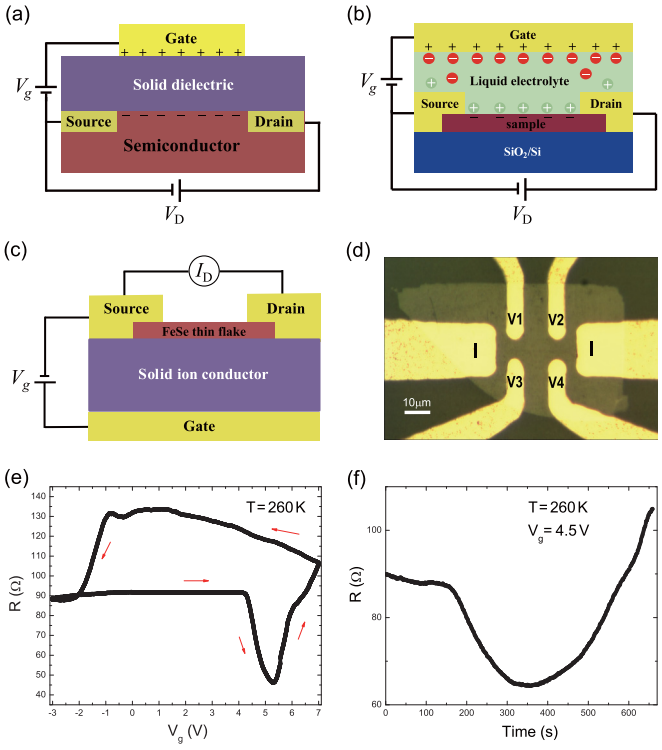

FIG. 1. Resistance controlled by gate voltage with the SIC-FET device. (a) A schematic illustration of a MISFET with a solid oxide such as SiO_2 or $SrTiO_3$ as the gate dielectric. (b) A schematic structure of EDL-FET with a liquid electrolyte as the gate dielectric. (c) A schematic diagram of a SIC-FET device with a solid ion conductor as the gate dielectric. (d) An optical image of a FeSe thin flake with a standard Hall bar configuration with the current and voltage terminals labeled. (e) Gate voltage dependence of the resistance for a FeSe thin flake with a typical thickness of about 18 nm in the SIC-FET device. The continuously swept gate voltage with a scan rate of 2 mV s^{-1} was applied at 260 K. (f) The evolution of resistance with time in SIC-FET with $V_g = 4.5$ V, where the resistance of the sample started to drop.

origin of superconductivity in these high-T_c materials remains an intriguing topic.

Recently, we have systematically tuned the superconductivity of FeSe thin flakes by electron doping with an EDL-FET device, and an onset T_c of 48 K was achieved [39]. However, the superconducting regime in the carrier-doping phase diagram is incomplete due to the sample damage caused by electrochemical reactions between samples and ionic liquids at a high gate voltage ($V_g > 6$ V). To investigate the whole superconducting regime, a more effective method is required to introduce a higher carrier density into FeSe.

Using the recently developed SIC-FET devices to increase electron doping in FeSe thin flakes by driving Li^+ into the samples, we have found structural transitions from the FeSe (11) phase to a low-doping $Li_yFe_2Se_2$ (122 phase-I), then to a high-doping 122 phase-II. A dome-shaped superconducting phase diagram was mapped out with increasing Li content, and T_c was enhanced from 8 K in FeSe to 46.6 K for optimal doping, then decreased in the overdoped regime, and eventually an insulating phase emerged. The SIC-FET device proves to be able to introduce a much higher carrier doping in bulk materials and stabilizes different structural phases.

We prepared FET devices with solid state lithium ion conductive glass ceramics as the gate dielectrics. The exfoliated FeSe thin flakes with a typical thickness of ~18 nm were used to fabricate the transport channel. Li^+ in the lithium ion conductor can move under an applied electric field. For a positive gate voltage, Li^+ accumulates on the surface of the samples, and then enters into the samples to tune the carrier concentration. Figure 1(c) depicts a schematic illustration of the SIC-FET device. Detailed device preparation procedures are described in the Supplemental Material [40]. Figure 1(d) shows the optical image of an FeSe thin flake with a standard Hall bar configuration and with the current and voltage terminals labeled. A typical R-V_g curve is shown in Fig. 1(e). The resistance of the FeSe thin flake remains almost unchanged with $V_g < 4.5$ V, and starts to drop quickly for $V_g > 4.5$ V, reaches a minimum at 5.3 V, and then increases rapidly. When the gate voltage is swept back to −2 V, the resistance can recover to the initial value. This behavior indicates that the tuning process is reversible.

In fact, as shown in Fig. 1(f), when the resistance of the sample starts to drop, the process of Li^+ intercalating into the FeSe thin flake sample will continue even if the gate voltage stays at a certain level. After intercalating Li^+ into FeSe thin flakes at 260 K, which is the optimal temperature for applying gate voltages, we quickly cooled down the FET devices to 200 K, below which the mobility of Li^+ in the lithium ion conductor is completely suppressed. The gate voltage of 4.5 V, at which the resistance of sample starts to drop, was kept unchanged during all measurements. In order to achieve a fine and systematic modulation of Li^+ intercalation, the FET device was relaxed at 260 K for a certain period of time before cooling down in each round. This procedure can lead to a series of doping levels with a controllable fashion.

Figure 2 shows the resistance of an FeSe thin flake with various amounts of intercalated Li^+. At $V_g = 0$ V, the sample

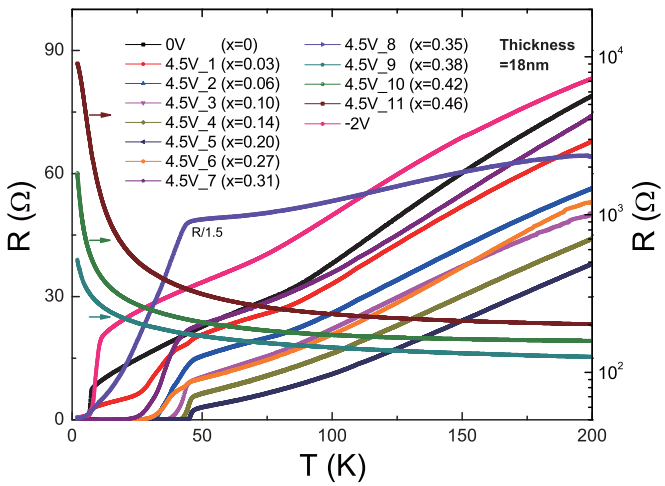

FIG. 2. Temperature dependence of resistance for a FeSe thin flake without gating and with a gate voltage $V_g = 4.5$ V. The thickness of the thin flake determined by atomic force microscopy is 18 nm. The x is the Li/Fe ratio whose determination is discussed in the Supplemental Material.

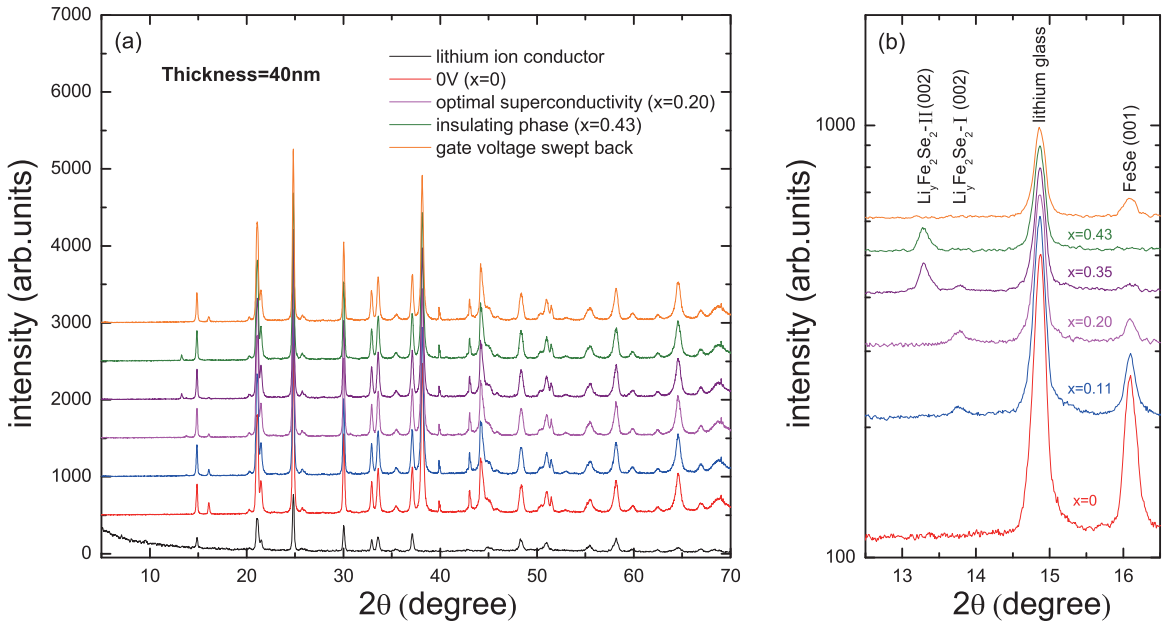

FIG. 3. *In situ* XRD patterns for an FeSe thin flake in the SIC-FET device before and after the intercalation of Li^+ ions. (a) Typical XRD patterns of FeSe thin flakes with a thickness of 40 nm for different charge stages. (b) A magnified view of the angle range from 12.5° to 16.5°.

is superconducting with an onset critical temperature $T_c^{\text{onset}} = 7.3$ K and reaches zero resistance at 5 K. Here, T_c^{onset} is defined as the intersection between the linear extrapolation of the normal state and the superconducting transition. By increasing the amount of intercalated Li^+, the electronic carrier density of the sample increases [as shown in Fig. S2(b) of the Supplemental Material [40]], and the T_c changes systematically as a function of Li^+ concentration. For the fifth round of cooling down at $V_g = 4.5$ V, the optimal superconductivity of the FeSe thin flake has been obtained with a Li/Fe ratio of 0.2. By further increasing the intercalated Li^+, the T_c starts to decrease, and eventually the FeSe thin flake shows an insulating behavior. When the gate voltage is swept back to −2 V, the resistance comes back to the initial value and the T_c also turns back to about 8 K, being almost the same as the initial T_c before gating. This behavior indicates that the carrier tuning procedure with the SIC-FET device is reversible. We note here that both the optimal $T_c^{\text{onset}} = 46.6$ K and the transition from the superconductivity to insulating behavior are highly repeatable in every measured device (more than 40 devices). The sample with optimal doping exhibits $T_c^{\text{onset}} = 46.6$ K and a zero-resistance temperature T_c^{zero} of 44.8 K, which is slightly higher than that of Li/ammonia intercalated FeSe compounds synthesized by the ammonothermal method [29]. The sharp transition width of ∼2 K is in striking contrast to that of ∼13 K observed in EDL-FET devices of FeSe thin flakes and thin films [39,41] (see Fig. S3 [40]), suggesting that the carrier concentration distribution in the SIC-FET devices is much more homogeneous.

Li^+ can be easily intercalated into layered materials by the electric field and alter the local crystal structures of the materials. Figure 3 shows *in situ* x-ray diffraction (XRD) patterns for a FeSe thin flake with a thickness of 40 nm before and after the intercalation of Li^+. Before the intercalation of Li^+, the diffraction peak of (001) appears at $2\theta = 16.09°$. By increasing the amount of intercalated Li^+, the (001) peak intensity shows a drastic decrease with no noticeable variation in position. The phase with an extremely low amount of Li^+ possesses the same structure as that of FeSe (11 phase), in which Li^+ diffuses randomly. With an increase of Li^+, two additional diffraction peaks appear at lower angles, 13.76° and 13.29°, indicating two different phases derived from the parent structure of FeSe. These peaks come from different phases because only the 13.29° peak shows up in the insulating phase [see Fig. 3(b)]. These two Li-intercalated FeSe phases are induced and stabilized by the SIC-FET device.

To identify these phases with stronger signals, we have also carried out XRD measurements on a thicker flake of 150 nm (see Fig. S4 in the Supplemental Material [40]). Two sets of (00l) diffraction peaks have been identified, suggesting that the separations between adjacent Fe layers (d) are 6.4128 and 6.6570 Å, respectively. In the $Na_{0.65}Fe_{1.93}Se_2$ and $K_xFe_{2-y}Se_2$ of a $ThCr_2Si_2$-type structure, the separations d are 6.8339 and 7.0180 Å, respectively [27,42]. Considering that the ionic radius of Li^+ is smaller than that of Na^+ and K^+, we attribute the two phases to the $ThCr_2Si_2$-type structure. We label the phase with a smaller d as the $Li_yFe_2Se_2$-I (122-I) phase and the one with a larger d as the $Li_yFe_2Se_2$-II (122-II) phase. The different layer separations d can be attributed to the different Li^+ contents. Generally speaking, the small cation may have more diverse arrangements and coordination environments. Similar multiple phases have been reported in Na-intercalated FeSe superconductors [42]. When the thin flake is tuned to an insulator, the 11 phase and 122-I phase completely disappear and only the 122-II phase exists, as shown in Fig. 3. When the gate voltage is swept back to −2 V, the 122-I and 122-II phases completely disappear, while the 11 phase recovers. These results indicate that the newly formed 122 structural phases can only exist under an electric field, and also imply

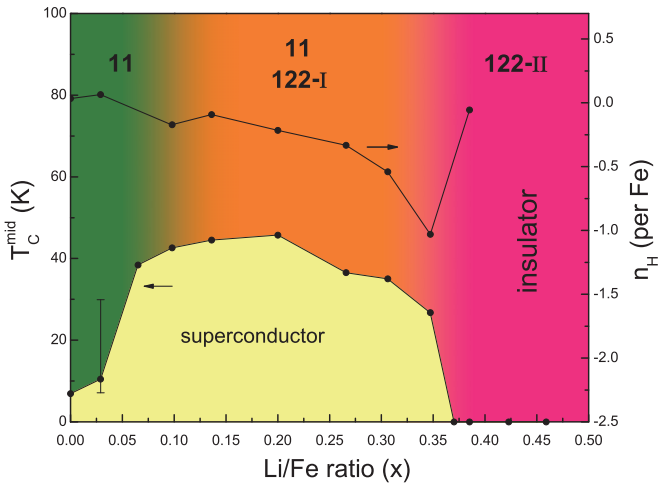

FIG. 4. The phase diagram of the Li-intercalated FeSe thin flake as a function of the Li/Fe ratio. The T_c shows a domelike behavior with increasing Li/Fe ratio. A phase transition from superconductor to insulator occurs around a Li/Fe ratio of 0.37. A series of structural phase transitions from the FeSe 11 phase to the $Li_yFe_2Se_2$-I phase, then to the $Li_yFe_2Se_2$-II phase, takes place. The Hall number n_H is plotted to show the variation in the effective carrier density.

that the process of intercalating Li^+ into the FeSe controlled by the electric field is reversible. We note that the coexistence of the 11, 122-I, and 122-II phases could be due to the inhomogeneous distribution of Li^+. Such an inhomogeneity strongly depends on the thickness of the FeSe thin flakes, which was confirmed by the XRD patterns shown in Fig. 3 and Fig. S4 [40] for thin flakes with different thicknesses. It should be pointed out that the data shown in Fig. 2 were obtained on FeSe thin flakes of 18 nm, which should be much more homogeneous than those observed in Fig. 3. It is possible that no coexistence of the 11, 122-I, and 122-II phases takes place in devices with flakes of 18 nm. We have tried to perform XRD measurements on a device with 18 nm thin flakes, but the sample was too thin to yield detectable signals. We thus selected 40 nm FeSe thin flakes for XRD characterization, which inevitably involves inhomogeneity. The evolution of these phases with Li^+ intercalation is summarized in Fig. 4.

To acquire more details about electron doping and structural modification, *in situ* x-ray photoelectron spectroscopy (XPS) and x-ray absorption near edge spectra (XANES) were performed on the SIC-FET devices and their results are shown in Figs. S5 and S6 [40]. The XPS for Fe $2p$ shows that the Fe valence state decreases with the increase in Li^+ intercalation (see the Supplemental Material [40]). In the XANES Fe K edge spectra, the main absorption feature is due to the transition from Fe $1s$ to the $4p$ state (see the Supplemental Material [40]). The absorption edge of the insulating phase shifts 2.5 eV towards lower energy relative to that of pure FeSe, corresponding to a change in the Fe valence state from +2 in the pure FeSe to 1.23 ± 0.15 in the insulating phase. Furthermore, the slight parallel shift of the absorption edge at the optimal superconducting state gives additional evidence for the random distribution of Li over Fe since a different local ordering may give rise to deviations in the absorption spectra. On the other hand, the distinct shift of the absorption edge in the insulating phase from that of the pure FeSe sample indicates a different ordering or structural change due to Li intercalation. Such a change is also responsible for the variation in the pronounced pre-edge feature at 7111 eV, which arises from the quadruple transition from Fe $1s$ to Fe $3d$. The decrease of the Fe valence state observed in both XPS and XANES suggests that Li^+ intercalation controlled by the electric field is an effective method to introduce electron carriers into the FeSe layers. The XANES measurements indicate that the Li^+ is randomly distributed in the 122-I phase, while it is ordered in the 122-II phase. Further investigation is required to determine the Li^+ positions and to reveal the microstructures of the two phases.

The phase diagram of superconductivity and the structural variations of Li^+-intercalated FeSe thin flakes are plotted as a function of the Li/Fe ratio in Fig. 4. To determine the amount of Li^+ in samples, we used a constant leakage current of 10 nA to control the intercalation process. The details are presented in the Supplemental Material [40]. By this means, the amount of Li^+ in the FeSe thin flakes only depends on the charge time. Optimal superconductivity is obtained when the resistance of the FeSe thin flake drops to the lowest point, and a Hall number of 0.20 per Fe site was determined by the averaged value from several samples. By taking the charge time and Li/Fe ratio of the optimal superconductivity as a reference, we can estimate the Li/Fe ratio in the thin flakes at different charge stages. As shown in Fig. 4, the T_c shows a domelike behavior with increasing intercalated Li^+. Optimal superconductivity with a midpoint critical temperature $T_c^{mid} = 45.8$ K has been achieved when the Li/Fe ratio reaches 0.2. As the ratio is increased to about 0.37, the superconductivity disappears completely, and then the sample becomes an insulator. A similar evolution from superconductor to insulator has been also observed in (Li,Fe)OHFeSe thin flakes by electric field controlled lithium doping [43]. Intriguingly, an abrupt jump in the T_c from ~10 to ~40 K is observed when the Li/Fe ratio is around 0.07. Meanwhile, the Hall number n_H shows a corresponding sudden sign reversal from a hole type to electron type, which can serve as an indication of a Lifshitz transition [44]. A similar transition has been observed in FeSe thin flakes with the EDL-FET device [39]. However, the effective carrier concentration introduced by Li^+ intercalation can further increase and go beyond the upper limit of EDL-FET devices. At a higher intercalation level, the carrier concentration suddenly decreases when the sample is tuned to an insulator, which could be attributed to some charge localization effect. Our XANES data suggest that Li ions are ordered in the insulating 122-II phase. How the FeSe layer becomes insulating and whether the ordering of Li ions is responsible for the nontrivial behavior in the FeSe layers require further investigation, which could be helpful in understanding the superconducting mechanism for FeSe-derived superconductors.

In summary, using a solid lithium ion conductor as the gate dielectric, we developed a FET device (SIC-FET), which can effectively tune the carrier concentration of layered materials by driving Li^+ in and out within a thickness of tens of nanometers. Compared to MIS-FET and EDL-FET devices, the SIC-FET device shows an improved capability of introducing charge carriers in solids, so that it can help to map out the phase diagram of FeSe over a wide range. Moreover, the SIC-FET device can be used to search for different

materials or superconductors with metastable structures. In particular, the configuration of SIC-FET devices is suitable for many surface-sensitive experimental examinations. Our studies demonstrate that the SIC-FET device can open a way to search for interesting electronic or structural phases, and potentially it can serve in modern electronic technology to some degree.

This work is supported by the National Natural Science Foundation of China (Grants No. 11190021, No. 11227902, No. 11534010, and No. 91422303), the Strategic Priority Research Program (B) of the Chinese Academy of Sciences (Grant No. XDB04040100), the National Key R&D Program of the MOST of China (Grant No. 2016YFA0300201), and the Hefei Science Center CAS (2016HSC-IU001).

[1] J. G. Bednoz and K. A. Müller, Z. Phys. B **64**, 189 (1986).
[2] Y. Kamihara, T. Watanabe, M. Hirano, and H. Hosono, J. Am. Chem. Soc. **130**, 3296 (2008).
[3] X. H. Chen, T. Wu, G. Wu, R. H. Liu, H. Chen, and D. F. Fang, Nature (London) **453**, 761 (2008).
[4] R. E. Glover, III and M. D. Sherrill, Phys. Rev. Lett. **5**, 248 (1960).
[5] C. H. Ahn, S. Gariglio, P. Paruch, T. Tybell, L. Antognazza, and J.-M. Triscone, Science **284**, 1152 (1999).
[6] D. Chiba, M. Yamanouchi, F. Matsukura, and H. Ohno, Science **301**, 943 (2003).
[7] C. H. Ahn, J. M. Triscone, and J. Mannhart, Nature (London) **424**, 1015 (2003).
[8] K. S. Novoselov, A. K. Geim, S. V. Morozov, D. Jiang, Y. Zhang, S. V. Dubonos, I. V. Grigorieva, and A. A. Firsov, Science **306**, 666 (2004).
[9] A. D. Caviglia, S. Gariglio, N. Reyren, D. Jaccard, T. Schneider, M. Gabay, S. Thiel, G. Hammerl, J. Mannhart, and J.-M. Triscone, Nature (London) **456**, 624 (2008).
[10] K. Ueno, S. Nakamura, H. Shimotani, A. Ohtomo, N. Kimura, T. Nojima, H. Aoki, Y. Iwasa, and M. Kawasaki, Nat. Mater. **7**, 855 (2008).
[11] K. Ueno, S. Nakamura, H. Shimotani, H. T. Yuan, N. Kimura, T. Nojima, H. Aoki, Y. Iwasa, and M. Kawasaki, Nat. Nanotechnol. **6**, 408 (2011).
[12] J. T. Ye, S. Inoue, K. Kobayashi, Y. Kasahara, H. T. Yuan, H. Shimotani, and Y. Iwasa, Nat. Mater. **9**, 125 (2010).
[13] A. T. Bollinger, G. Dubuis, J. Yoon, D. Pavuna, J. Misewich, and I. I. Božović, Nature (London) **472**, 458 (2011).
[14] J. T. Ye, Y. J. Zhang, R. Akashi, M. S. Bahramy, R. Arita, and Y. Iwasa, Science **338**, 1193 (2012).
[15] Y. J. Yu, F. Y. Yang, X. F. Lu, Y. J. Yan, Y.-H. Cho, L. G. Ma, X. H. Niu, S. Kim, Y.-W. Son, D. L. Feng, S. Y. Li, S.-W. Cheong, X. H. Chen, and Y. B. Zhang, Nat. Nanotechnol. **10**, 270 (2015).
[16] Y. Saito, Y. Kasahara, J. T. Ye, Y. Iwasa, and T. Nojima, Science **350**, 409 (2015).
[17] J. M. Lu, O. Zheliuk, I. Leermakers, N. F. Q. Yuan, U. Zeitler, K. T. Law, and J. T. Ye, Science **350**, 1353 (2015).
[18] L. J. Li, E. C. T. O'Farrell, K. P. Loh, G. Eda, B. Özyilmaz, and A. H. Castro Neto, Nature (London) **529**, 185 (2016).
[19] B. Radisavljevic, A. Radenovic, J. Brivio, V. Giacometti, and A. Kis, Nat. Nanotechnol. **6**, 147 (2011).
[20] L. K. Li, Y. J. Yu, G. J. Ye, Q. Q. Ge, X. D. Ou, H. Wu, D. L. Feng, X. H. Chen, and Y. B. Zhang, Nat. Nanotechnol. **9**, 372 (2014).
[21] C. H. Ahn, A. Bhattacharya, M. Di Ventra, J. N. Eckstein, C. D. Frisbie, M. E. Gershenson, A. M. Goldman, I. H. Inoue, J. Mannhart, A. J. Millis, A. F. Morpurgo, D. Natelson, and J.-M. Triscone, Rev. Mod. Phys. **78**, 1185 (2006).
[22] K. Ueno, H. Shimotani, H. T. Yuan, J. T. Ye, M. Kawasaki, and Y. Iwasa, J. Phys. Soc. Jpn. **83**, 032001 (2014).
[23] H. T. Yuan, H. Shimotani, A. Tsukazaki, A. Ohtomo, M. Kawasaki, and Y. Iwasa, Adv. Funct. Mater. **19**, 1046 (2009).
[24] J. Jeong, N. Aetukuri, T. Graf, T. D. Schladt, M. G. Samant, and S. S. P. Parkin, Science **339**, 1402 (2013).
[25] T. D. Schladt, T. Graf, N. B. Aetukuri, M. Li, A. Fantini, X. Jiang, M. G. Samant, and S. S. Parkin, ACS Nano **7**, 8074 (2013).
[26] F. C. Hsu, J. Y. Luo, K. W. Yeh, T. K. Chen, T. W. Huang, P. M. Wu, Y. C. Lee, Y. L. Huang, Y. Y. Chu, D. C. Yan, and M. K. Wu, Proc. Natl. Acad. Sci. USA **105**, 14262 (2008).
[27] J. G. Guo, S. F. Jin, G. Wang, S. C. Wang, K. X. Zhu, T. T. Zhou, M. He, and X. L. Chen, Phys. Rev. B **82**, 180520(R) (2010).
[28] A. F. Wang, J. J. Ying, Y. J. Yan, R. H. Liu, X. G. Luo, Z. Y. Li, X. F. Wang, M. Zhang, G. J. Ye, P. Cheng, Z. J. Xiang, and X. H. Chen, Phys. Rev. B **83**, 060512(R) (2011).
[29] M. Burrard-Lucas, D. G. Free, S. J. Sedlmaier, J. D. Wright, S. J. Cassidy, Y. Hara, A. J. Corkett, T. Lancaster, P. J. Baker, S. J. Blundell, and S. J. Clarke, Nat. Mater. **12**, 15 (2013).
[30] X. F. Lu, N. Z. Wang, H. Wu, Y. P. Wu, D. Zhao, X. Z. Zeng, X. G. Luo, T. Wu, W. Bao, G. H. Zhang, F. Q. Huang, Q. Z. Huang, and X. H. Chen, Nat. Mater. **14**, 325 (2015).
[31] Q. Y. Wang, Z. Li, W. H. Zhang, Z. C. Zhang, J. S. Zhang, W. Li, H. Ding, Y. B. Ou, P. Deng, and K. Chang, Chin. Phys. Lett. **29**, 037402 (2012).
[32] D. F. Liu, W. H. Zhang, D. X. Mou, J. F. He, Y. B. Ou, Q. Y. Wang, Z. Li, L. L. Wang, L. Zhao, S. L. He, Y. Y. Peng, X. Liu, C. Y. Chen, L. Yu, G. D. Liu, X. L. Dong, J. Zhang, C. T. Chen, Z. Y. Xu, J. P. Hu, X. Chen, X. C. Ma, Q. K. Xue, and X. J. Zhou, Nat. Commun. **3**, 931 (2012).
[33] S. L. He, J. F. He, W. H. Zhang, L. Zhao, D. F. Liu, X. Liu, D. X. Mou, Y. B. Ou, Q. Y. Wang, Z. Li, L. L. Wang, Y. Y. Peng, Y. Liu, C. Y. Chen, L. Yu, G. D. Liu, X. L. Dong, J. Zhang, C. T. Chen, Z. Y. Xu, X. Chen, X. C. Ma, Q. K. Xue, and X. J. Zhou, Nat. Mater. **12**, 605 (2013).
[34] S. Y. Tan, Y. Zhang, M. Xia, Z. R. Ye, F. Chen, X. Xie, R. Peng, D. F. Xu, Q. Fan, H. C. Xu, J. Jiang, T. Zhang, X. C. Lai, T. Xiang, J. P. Hu, B. P. Xie, and D. L. Feng, Nat. Mater. **12**, 634 (2013).
[35] R. Peng, H. C. Xu, S. Y. Tan, H. Y. Cao, M. Xia, X. P. Shen, Z. C. Huang, C. H. P. Wen, Q. Song, T. Zhang, B. P. Xie, X. G. Gong, and D. L. Feng, Nat. Commun. **5**, 5044 (2014).
[36] J. F. Ge, Z. L. Liu, C. H. Liu, C. L. Gao, D. Qian, Q. K. Xue, Y. Liu, and J. F. Jia, Nat. Mater. **14**, 285 (2015).
[37] L. Zhao, A. J. Liang, D. N. Yuan, Y. Hu, D. F. Liu, J. W. Huang, S. L. He, B. Shen, Y. Xu, X. Liu, L. Yu, G. D. Liu, H. X. Zhou, Y. L. Huang, X. L. Dong, F. Zhou, K. Liu, Z. Y. Lu, Z. X. Zhao, C. T. Chen, Z. Y. Xu, and X. J. Zhou, Nat. Commun. **7**, 10608 (2016).

[38] X. H. Niu, R. Peng, H. C. Xu, Y. J. Yan, J. Jiang, D. F. Xu, T. L. Yu, Q. Song, Z. C. Huang, Y. X. Wang, B. P. Xie, X. F. Lu, N. Z. Wang, X. H. Chen, Z. Sun, and D. L. Feng, Phys. Rev. B **92**, 060504(R) (2015).

[39] B. Lei, J. H. Cui, Z. J. Xiang, C. Shang, N. Z. Wang, G. J. Ye, X. G. Luo, T. Wu, Z. Sun, and X. H. Chen, Phys. Rev. Lett. **116**, 077002 (2016).

[40] See Supplemental Material at http://link.aps.org/supplemental/10.1103/PhysRevB.95.020503, which includes Refs. [11,39,41,45–48], for more details about the preparation of SIC-FET devices and characterization of Li^+-intercalated FeSe thin flakes.

[41] K. Hanzawaa, H. Satoa, H. Hiramatsua, T. Kamiyaa, and H. Hosono, Proc. Natl. Acad. Sci. USA **113**, 3986 (2016).

[42] J. G. Guo, H. C. Lei, F. Hayashi, and H. Hosono, Nat. Commun. **5**, 4756 (2014)

[43] B. Lei, Z. J. Xiang, X. F. Lu, N. Z. Wang, J. R. Chang, C. Shang, A. M. Zhang, Q. M. Zhang, X. G. Luo, T. Wu, Z. Sun, and X. H. Chen, Phys. Rev. B **93**, 060501(R) (2016).

[44] I. M. Lifshitz, Sov. Phys. JETP **11**, 1130 (1960).

[45] H. C. Lei, D. Graf, R. W. Hu, H. Ryu, E. S. Choi, S. W. Tozer, and C. Petrovic, Phys. Rev. B **85**, 094515 (2012).

[46] W. H. Zhang, Z. Li, F. S. Li, H. M. Zhang, J. P. Peng, C. J. Tang, Q. Y. Wang, K. He, X. Chen, L. L. Wang, X. C. Ma, and Q. K. Xue, Phys. Rev. B **89**, 060506(R) (2014).

[47] X. D. Qi, J. Y. Wang, J. C. Kuo, K. A. Yates, and L. F. Cohen, J. Alloys Compd. **509**, 6350 (2011).

[48] N. S. McIntyre and D. G. Zetaruk, Anal. Chem. **49**, 1521 (1977).